Locally controlled Cu-ion transport in layered ferroelectric $CuInP_2S_6$

Nina Balke[1*], Sabine M. Neumayer[1,2], John A. Brehm[3], Michael A. Susner[4,5,6], Brian J. Rodriguez[2], Stephen Jesse[1], Sergei V. Kalinin[1], Sokrates T. Pantelides[3,4], Michael A. McGuire[4], Petro Maksymovych[1*]

[1]Center for Nanophase Materials Sciences, Oak Ridge National Laboratory, 1 Bethel Valley Rd. Oak Ridge, TN 37831, USA

[2]School of Physics, University College Dublin, Belfield, Dublin 4, Ireland

[3]Department of Physics & Astronomy, Vanderbilt University, Box 1807-B, 6631 Stevenson Center, Nashville, TN 37235

[4]Materials Science and Technology Division, Oak Ridge National Laboratory, 1 Bethel Valley Rd. Oak Ridge, TN 37831, USA

[5]Aerospace Systems Directorate, Air Force Research Laboratory, 1950 Fifth Street, Bldg. 18 Wright-Patterson Air Force Base, OH 45433, USA

[6]UES, Inc., 4401 Dayton-Xenia Road. Beavercreek, OH 45432, USA

*Corresponding authors: Nina Balke (balken@ornl.gov), Petro Maksymovych (maksymovychp@ornl.gov)

Keywords: Transition-metal chalcogenophosphate, copper indium thiophosphate, layered ferroelectric, ionic transport, scanning probe microscopy

Abstract

Metal thiophosphates are attracting growing attention in the context of quasi-2D van-der-Waals functional materials. Alkali thiophosphates are investigated as ion conductors for solid electrolytes and transition metal thiophosphates are explored as new class of ferroelectric materials. For the latter, a representative copper indium thiophosphate is ferrielectric at room temperature, and despite low polarization exhibits giant negative electrostrictive coefficients. Here, we reveal that ionic conductivity in this material enables localized extraction of Cu-ions from the lattice with a biased scanning probe microscopy tip, that is surprisingly reversible. The ionic conduction is tracked through local volume changes with a scanning probe microscopy tip providing a current-free probing technique which can be explored for other thiophosphates of interest. Nearly 90nm tall crystallites can be formed and erased reversibly on the surface of this material as result of ionic motion, the size of which can be sensitively controlled by both magnitude and frequency of the electric field, as well as the ambient temperature. These experimental results and density functional theory calculations point to a remarkable resilience of $CuInP_2S_6$ to large scale ionic displacement and Cu-vacancies, in part enabled by metastability of Cu-deficient phases. Furthermore, we have found that piezoelectric response of $CuInP_2S_6$ is enhanced by about 45% when a slight ionic modification is carried out with applied field. This new mode of modifying the lattice of $CuInP_2S_6$, and more generally ionically conducting thiophosphates, posits new prospects for their applications in van-der-Waals heterostructures, possibly in the context of catalytic or electronic functionalities.

Introduction

Recently, attention has been drawn to several members of layered transition-metal chalcogenophosphates, with a general formula of $M^{1+}M^{3+}P_2Q_6$ or $M_2^{2+}P_2S_6$ (Q=S,Se).[1] These materials can be thought of as structural analogues of metal dichalcogenides, but with 1/3 of the metal atoms replaced by a diphoshphorus entity (P-P), which binds six adjacent sulfur atoms into $[P_2S_6]^{4-}$ anion. The increased ionicity of the bonding as well as the low oxidation state of transition metal ions may lead to ferroelectric ordering, as is the exemplary case of $CuInP_2S_6$ (CIPS) below 310K.[2-5] Therefore, thiophosphates are candidate materials to introduce polarization switching, piezoelectricity, dielectric tunabilitiy[3, 6-8] and more generally structural correlations into the paradigm of 2D materials and van-der-Waals heterostructures.[1, 9] Just above the ferroelectric transition temperature, giant electrostriction – a signature property of CIPS – is preserved, and the lattice, therefore, exhibits pronounced field-induced and continuously-tunable expansion.[10] It is also known, from macroscopic measurements, that CIPS attains significant ionic conductivity.[11] Because of this, thiophosphates featuring the $[P_2S_6]^{4-}$ anion are also considered as solid electrolyte for Li- and Na-ion batteries.[12-17] It is presently unclear, however, how localized information about ionic transport properties can be obtained and if ionic conductivity is compatible with other bias-induced functional material parameters such as piezoelectricity and dielectric tunability. Moreover, ionic conductivity implies the existence and stability of transition states, where 1) ions are displaced significantly away from their equilibrium positions, and 2) lattice vacancies (transient or permanent) are created. However, there are currently no atomistic mechanisms proposed for ionic conductivity in transition metal thiophosphates, including such properties as vacancy energetics.[1] Here, we use scanning probe microscopy (SPM) to study ionic transport in CIPS as a function of temperature, utilizing the

coupling between ionic motion and volume change as an observable to detect and quantify ionic processes. This concept has been introduced as Electrochemical Strain Microscopy (ESM)[18] to study localized ionic transport which is initiated by a biased sharp metal tip of about 30nm radius in contact with the surface which we adapt for thiophosphates. This approach can be universally applied to other metal thiophosphates to study the local ionic conduction properties and visualize local variations with 10's of nm lateral resolution. We also believe that electrochemical modification of thiophosphate surfaces open new possibilities for nanostructuring of materials in this family, toward local modification of their properties as well as interfaces with other electronic materials. For that reason, the study of ion conduction is performed on a ferrielectric thiophosphate.

Experimental Section

Measurements were conducted on a multiphase CIPS/IPS sample of several μm thickness that was prepared as described elsewhere.[10] The sample was mounted on a copper substrate with conductive silver paint. Before measurements, the sample was cleaved in an Ar filled glove box to obtain a clean surface.

All SPM measurements were performed in a protective Ar environment in a glove box with a Bruker Icon SPM equipped with a heater stage. Displacement was measured by the z-position of a SPM cantilever in contact with the sample surface while electric fields were applied. Baseline correction was needed to account for drift and was performed so that the minimum cantilever displacement is zero. For most measurements, additional ac voltages were applied in addition to the dc voltage sweep to access information about contact resonance frequency and material

responses to ac fields. This was done utilizing the band excitation (BE) technique which was also used to measure hysteresis loops measurements at room temperature. All ac voltages applied were $1V_{ac}$. The cantilever used for all studies was Nanosensor PPP-EFM with a typical free resonance of 75kHz and a typical force constant of 3N/m. All but the frequency-dependent measurements were performed on a 30x30 point grid across a 5μm x 5μm area. The bias-induced electromechanical response of the CIPS and IPS phase were analyzed separately by using PCA component analysis to create mask and average responses are shown. The frequency-dependent measurements were performed in a single location for each frequency and multiple curves were analyzed. PFM imaging was performed at a single frequency close to the contact resonance frequency with the help of a function generator and an external lock-in.

Results and Discussion

We briefly recount the basic properties of CIPS and the SPM methods used in this work. Measurements were performed on heterostructured crystals comprising CIPS and vacancy-ordered $In_{4/3}P_2S_6$ (IPS) phases.[6] The average composition of the crystal was $Cu_{0.4}In_{1.2}P_2S_6$ with a Curie temperature of 340K. While CIPS is ferrielectric and exhibits giant negative electrostrictive coefficients that lead to large electromechanical displacement despite small intrinsic polarization values[10] of only a few $\mu C/cm^2$ IPS is Cu-free and non-ferroelectric. The comparison of the two phases, therefore, allows us to assess Cu ion mobility in the CIPS phase[19], whereas the IPS phase additionally provides a reference for measurements related to ionic conductivity.

Piezoresponse force microscopy (PFM) at room temperature (RT) clearly reveals the existence of the ferrielectric CIPS and non-ferroelectric IPS phases– white and grey stripes, correspondingly in (Figure 1a). At a temperature of 363K, well above the Curie temperature, the PFM contrast mostly disappears and the PFM amplitude of the CIPS phase is strongly reduced, and becomes largely equivalent to that of non-ferroelectric IPS as previously observed (Figure 1b).[10] The residual response can be explained by electrostatic forces between the biased SPM tip and sample surface, electrochemical strain caused by ionic motion, or electrostriction which can still exist in the paraelectric state.

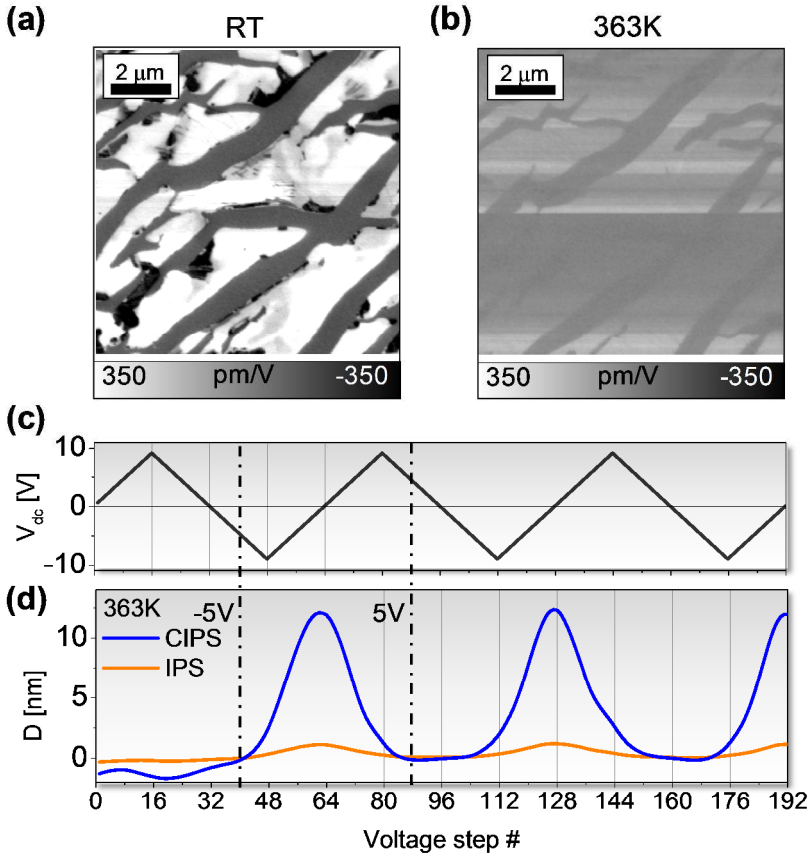

Figure 1: PFM images measured near the contact resonance frequency at RT (a) and 363K (b). Applied dc voltage profile (c) and corresponding averaged cantilever displacement D (d) at 363K for the CIPS and IPS phases as function of time. The effective cycling frequency was 2 Hz.

The field-induced electromechanical response in the paraelectric state at 363K was mapped across a 5μm x 5 μm area and inferred from the recorded z-displacement (D) of the metal tip caused by applied electric field and measured under a constant contact force between SPM probe and sample surface. The applied triangular voltage waveform, the averaged responses for CIPS and IPS are shown in Fig. 1c,d. This characterization mode is analog to static ESM where only DC voltages are applied to the tip. In traditional ESM,[18] dynamic strain changes are investigated as function of DC voltage to take advantage of resonance enhancement for better signal to noise ratio.

For pristine surfaces, a positive voltage has little effect (steps 0-32). However, at negative voltage polarity, the surface begins to expand very dramatically. After application of -5V surface topography starts to expand and continues to do so until the voltage is reversed back to 0 V (steps 40-64), as seen from the measured change of the surface height relative to its original value (D). Reverting the voltage polarity to positive causes the expanded surface height to decrease (steps 64-80), and almost completely reset back to the original starting value (Fig. 1c,d). After the initial cycling, the surface displacement profile is repeatable and reversible over all subsequent voltage cycles. The resulting displacement curves are bell-shaped when plotted against the voltage and feature one high displacement branch and one zero-displacement branch (Fig. 2a). The derivative of the displacement curve $\delta D/\delta V$ clearly shows the voltage threshold for induced surface deformation (at ~ 5V), its metastability down to 0 V and reversibility at approximately the same voltage of opposite polarity (~-5V) as displayed in Fig. 2a. The overall

derivative characteristic is qualitatively reminiscent of current-voltage characteristics of a memristor, whose function is based on metastable electronic states.[20] The map of the maximum displacement ΔD measured at the remnant state at zero V_{dc} (Fig. 2b) further reveals that IPS phase displays only very small changes in displacements, highlighting the fact that the presence of Cu is required for large volume changes. The maximum displacement ΔD measured at 363K with the voltage profile measured at a frequency of 2Hz is on average 12 nm in comparison to the c lattice spacing of about 13.25Å.[6] If we assume that the main material probing depth is about the order of the tip radius of 30nm (which is typically a good assumption for SPM), we obtain an estimate of nominal strain of 40%. Of course, this estimate might be too simplified without considering the actual field distribution within the material but gives a good estimate on the extraordinary electromechanical sample response based on ionic motion. Given that ionic motion is a relatively slow and thermally activated process, the clear signature of the involvement of ionic diffusion is the dependence of the observables on the measurement temperature and the frequency of the driving field. Figure 2c shows this maximum reversible displacement as functions of temperature separated into the response from the CIPS and IPS phase. As characteristic for ion diffusion processes, the displacement increases with increasing temperature. Below the Curie temperature of 310K, no significant displacement can be measured, which suggests that ionic motion is minimal or even non-existent for this material at room temperature (Figure S1). The corresponding Arrhenius plots allow us to derive activation energy for Cu-ion motion 0.71eV (Figure 2c). The effect of frequency on the maximum displacement ΔD at a temperature of 363K is displayed in Figure 2d. At low frequencies, the response is large reaching almost 100nm for frequencies as low as 100mHz. With increasing frequency, the response drops until it is below the noise level for frequencies higher than10 Hz.

The shape profile of the maximum displacement as function of frequency (Figure 2d) is very characteristic and has been theoretically predicted for the frequency-dependent ESM signal based on ionic motion.[21-23] The corresponding displacement loops can be found in Figure S2. Interestingly, the IPS phase without Cu-ions also shows some small displacement at higher temperatures (Figure S1) with a different activation energy of 0.61 eV (Figure 2c). This means, ions other than Cu, such as P or S can contribute to the measured ion displacement measured on the CIPS phase. However, the displacement is so small that it falls within the error of the activation energy of the Cu-ion motion.

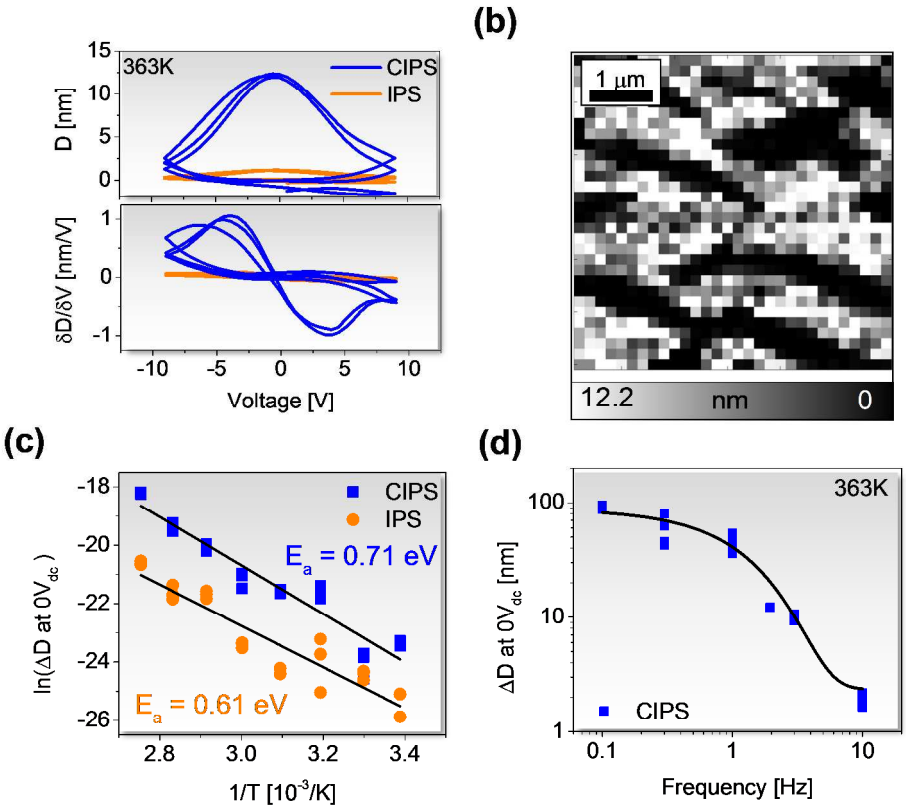

Figure 2: (a) Displacement D and derivative of displacement δD/δV at 363K separated and averaged for CIPS and IPS phase as function of applied dc voltage. The effective cycling frequency was 2Hz. (b) Corresponding spatially resolved map of maximum displacement ΔD. Analysis of reversible displacement ΔD at zero voltage for CIPS and IPS phase as function of temperature (c) and dc voltage sweep frequency (d).

A number of previous works alluded to the possibility of observing large local lattice strains due to ionic motion in the confined electric field of the SPM tip. Qualitatively, the detailed origins of the strain fall into one of two categories:

1) Electrochemical strain where the unit cell volume depends on the ion concentration. In this case, ions are moved by the local electric field resulting in a local volume change. The implicit assumption here is that ions displace beyond a unit cell but remain confined in the crystal lattice. This mechanism was suggested as a SPM-based probe methodology for battery materials under the term of electrochemical strain microscopy (ESM).[24-33]

2) Local electrodeposition driven by the current provided through the SPM tip resulting in additional material volume on the surface. This method has been shown for solid electrolytes used in Li-ion batteries[34-36] for irreversible processes and Ag ion conducting solid electrolyte glasses where particle growth can be reversible.[37, 38]

We posited above that the diffusion of Cu-cations from their normal positions is the likeliest explanation of the observed electromechanical response in CIPS. We hypothesize that atoms are eventually extracted out of the lattice and deposited as Cu crystallites on the surface. The negative probe bias required to trigger the process and initiate deposition (Cu^{+1} reduction) and

the positive bias required to dissolve the ions (Cu oxidation) are further consistent with this picture. The lack of significant response from $In_{4/3}P_2S_6$ phase yet again confirms that Cu^{+1} must be involved. An important question is the composition of the Cu-deficient $CuInP_2S_6$ formed by Cu^{+1} depletion from the volume. While in $RbAg_4I_5$ and $(AgI)_{0.25}$ $(AgPO_3)_{0.75}$ glasses, charge neutrality is fulfilled by replenishment of ions from the Ag counter electrode,[37, 38] the bottom electrode used in this study is silver paint and does not provide Cu ions, ruling out a similar mechanism. Therefore, to maintain electroneutrality, extraction of Cu^{+1} requires additional oxidation of the residual atoms in the lattice.

For a composition of $Cu_{0.5}InP_2S_6$, the oxidation state of Cu will need to formally increase to Cu^{+2}. To this end, we have calculated the stability of $Cu_{0.5}InP_2S_6$ by DFT, with the structure shown in Figure 3. The structure is metastable, with no negative-frequency phonons, and, in terms of Gibbs free energy, is 2.03eV/uc less stable than $CuInP_2S_6$. However, perhaps the most notable difference is that $Cu_{0.5}InP_2S_6$ is centrosymmetric, with Cu in the middle of the layers most likely due to the changes in the stereochemical interactions between Cu^{+2} and sulfur sublattice. Complete removal of Cu leads to unstable InP_2S_6 structure, as expected. The stable electroneutral composition is $In_{4/3}P_2S_6$ (IPS) to maintain a formal charge of no more than +3 on the indium atom. Naturally, we do not need to limit the consideration of possible structures to fully oxidized compounds. For example, a likely scenario is just introduction of dilute Cu vacancy concentration in our experiment. From DFT we estimate a cost of ~ 1eV per Cu vacancy in this compound. The high tolerance of $CuInP_2S_6$ toward Cu vacancies, and the possibility to reversibly changes its composition in electric field is really encouraging for potential consideration of the use of this material in a variety of ionic applications.

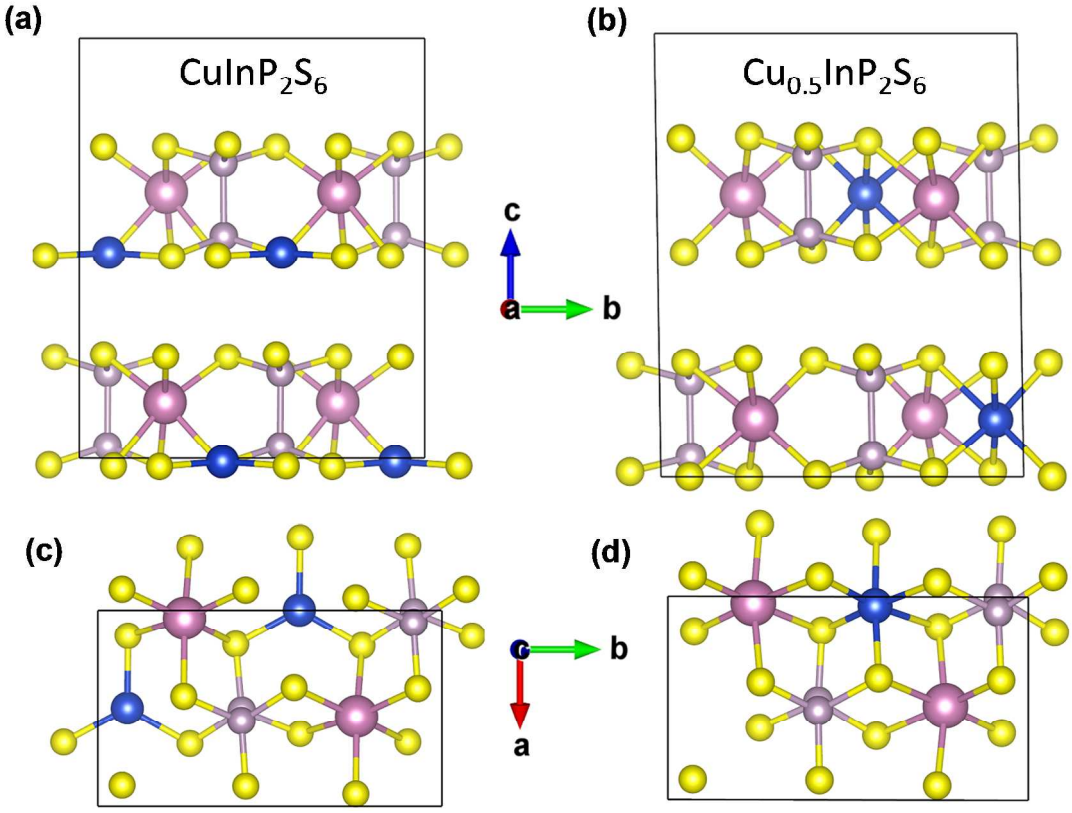

Figure 3. Structures of CuInP2S6 (a,c) and $Cu_{0.5}InP_2S_6$ (b,d) obtained by DFT, viewed along the a-axis (a,b) and c-axis (c,d), respectively. The unit-cells are shown as black boxes. Note the

centrosymmetric position of Cu in $Cu_{0.5}InP_2S_6$, unlike a strongly offset position of Cu in $CuInP_2S_6$.

Due to the large remnant displacement visible at zero V_{dc} (Figure 2a) it is to be expected that there are remnant changes in the sample topography if the applied voltage profile ends after application of negative voltages (Figure 1c). This has been observed through topography scans after the measurements were performed on a grid (Figure 4a). The IPS phase does not show any topography changes. Moreover, the changes observed for CIPS are sufficiently long-lived, so that they persist even after cooling the sample to room temperature.

It is natural to ask whether the ferroelectric properties of $CuInP_2S_6$ can be influenced by metal-ion extraction and a corollary injection of Cu-vacancies. According to DFT, the hypothetical $Cu_{0.5}InP_2S_6$ is centrosymmetric, so it should have no piezoelectric response. However, at smaller vacancy density, the strain and electrostatic dipoles may well affect the behavior $CuInP_2S_6$. Given that such configurations are not computationally accessible at the moment, a direct experimental probe is desired. We therefore directly measured the ferroelectric properties of the modified and unmodified $CuInP_2S_6$ using Band Excitation PFM voltage spectroscopy.[39-41]

As seen in Figure 4, in the area with topographic changes (region 1) ferroelectric hysteresis loops were increased in size, indicating larger electromechanical response. The change is quite pronounced, with about 45% stronger electromechanical response, compared to the as-grown state (region 2, Figure 4b). The change in ferroelectric properties is also visible in the on-field ferroelectric hysteresis (Figure S3a). The other detected change is a slight increase in contact resonance frequency (Figure S3b) after surface modification, implying a change of contact area

between tip and sample or mechanical sample properties. However, the electromechanical response is not generally dependent on the contact area, while band-excitation efficiently decouples the local changes in the contact stiffness, allowing systematic comparison of the electromechanical response.

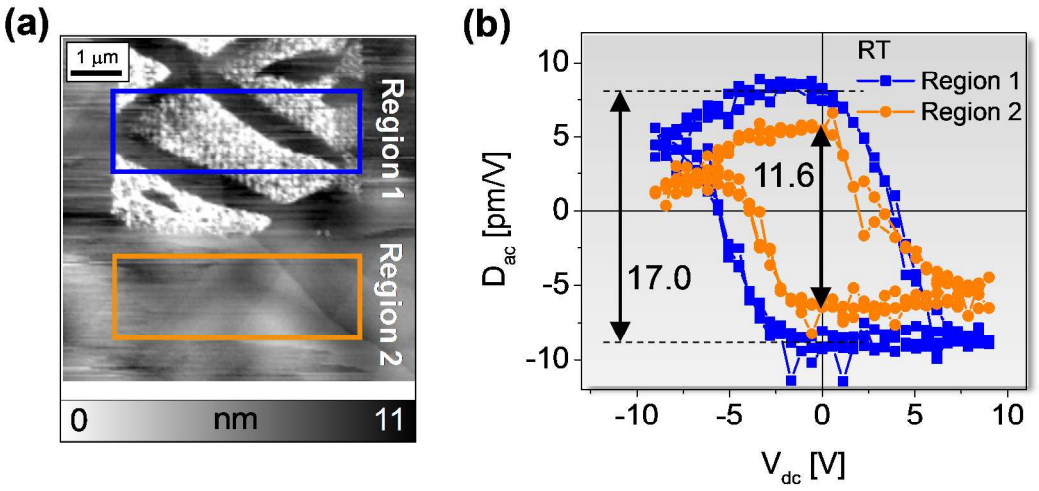

Figure 4: Effect of the topographical changes (a) on room temperature ferroelectric hysteresis loops averaged over the ferroelectric CIPS phase in region 1 and 2 (b).

We would like to emphasize, that CIPS by itself has anomalous large piezoelectric coefficient, comparable to the best oxide ferroelectrics. Although the spontaneous polarization is small, a large piezoelectric coefficient stems from a giant electrostrictive coefficient, which is 100-fold larger than in perovskite oxides and is second only to polymers and foams. A further increase of this value by Cu-vacancy injection is certainly very encouraging, particularly that these values can be stabilized for prolonged periods of times and are themselves reversible. A possible explanation here is that the properties of $CuInP_2S_6$ are modulated by strain dipoles due to Cu vacancies in the lattice, or Cu present in the van-der-Waals gap.

Conclusion

Strain-based detection of ionic mobility in solid state materials offers insight into local ionic processes which can be universally applied to many different material systems. In the case of quasi-2D layered CIPS, reversible large electromechanical deformation up to several 10s of nm caused by ionic motion were observed. The resulting sample surface displacement depends on the rate, magnitude, and history of the applied bias and is metastable – meaning that the shape of the surface can be controlled by appropriate voltage waveforms. The displacement increases with increasing temperature and decreasing frequency (with a maximum value of ~90nm observed at 100mHz and 363K), characteristic of ionic motion as the mechanism. Direct comparison to Cu-free IPS phase unambiguously identifies mobile Cu ions in CIPS as the primary reason for the observed surface deformation in this material. We inferred that displacement, extraction, and reduction of Cu-cations toward Cu-crystallites is basic mechanism for the morphological changes in the probed volume. This mechanism also implies the high tolerance of $CuInP_2S_6$ to cation off-stoichiometry. DFT calculations imply metastability of Cu-deficient compositions down to 50% ($Cu_{0.5}P_2S_6$) and a cost of ~ 1eV per Cu^{+1} vacancy. This possibility to move between Cu^{+1} and Cu^{2+} valency through extraction and reinsertion of Cu makes CIPS a promising ionic conductor material. Moreover, we measured an enhanced piezoelectric response taken in vacancy-rich areas, indicating that there exists a possibility to tailor the electromechanical behaviour at room temperature through the introduction of Cu-vacancies.

Finally, the tuneable surface deformation in CIPS at $T>T_C$ provides interesting prospects for applications in actuators, sensors and electronic applications as well as the possibility to modify room temperature electromechanical responses.

Author Contribution

The experiments were designed and conducted by NB, SNM and PM. The samples were synthesized by MAS and MAM. DFT calculations were performed by JAB. The software for SPM-based measurements was programmed by SJ. The manuscript was written through contributions of all authors. All authors have given approval to the final version of the manuscript.

Acknowledgement

The experimental work was supported by the Division of Materials Sciences and Engineering, Basic Energy Sciences, Department of Energy. The experiments were conducted at the Center for Nanophase Materials Sciences, which is a DOE Office of Science User Facility. Partial support for SPM-based experiments was provided by a research grant from Science Foundation (SFI) under the US-Ireland R&D Partnership Programme Grant Number SFI/14/US/I3113. Material synthesis was supported by the Air Force Research Laboratory under an Air Force Office of Scientific Research grant (LRIR No. 14RQ08COR) and a grant from the National Research Council.

Supporting Information description

The supporting information contains additional information about the change in electromechanical response of CIPS and IPS as function of temperature and frequency as well as additional results of the effect on electrochemically modified surfaces on ferroelectric properties at room temperature. This material is available free of charge via the Internet at http://pubs.acs.org.

References

(1) Susner, M. A.; Chyasnavichyus, M.; McGuire, M. A.; Ganesh, P.; Maksymovych, P. Metal Thio□and Selenophosphates as Multifunctional Van Der Waals Layered Materials Adv. Mater. 2017, 29, 1602852.

(2) Simon, A.; Ravez, J.; Maisonneuve, V.; Payen, C.; Cajipe, V. B. Paraelectric Ferroelectric Transition in the Lamellar Thiophosphate Cuinp2s6 Chem. Mater. 1994, 6, 1575-1580.

(3) Belianinov, A.; He, Q.; Dziaugys, A.; Maksymovych, P.; Eliseev, E.; Borisevich, A.; Morozovska, A.; Banys, J.; Vysochanskii, Y.; Kalinin, S. V. Cuinp2s6 Room Temperature Layered Ferroelectric Nano Lett. 2015, 15, 3808-3814.

(4) Liu, F. C.; You, L.; Seyler, K. L.; Li, X. B.; Yu, P.; Lin, J. H.; Wang, X. W.; Zhou, J. D.; Wang, H.; He, H. Y.; Pantelides, S. T.; Zhou, W.; Sharma, P.; Xu, X. D.; Ajayan, P. M.; Wang, J. L.; Liu, Z. Room-Temperature Ferroelectricity in Cuinp2s6 Ultrathin Flakes Nat. Commun. 2016, 7.

(5) Song, W. S.; Fei, R. X.; Yang, L. Off-Plane Polarization Ordering in Metal Chalcogen Diphosphates from Bulk to Monolayer Phys. Rev. B 2017, 96.

(6) Susner, M. A.; Belianinov, A.; Borisevich, A.; He, Q.; Chyasnavichyus, M.; Demir, H.; Sholl, D. S.; Ganesh, P.; Abernathy, D. L.; McGuire, M. A. High-T C Layered Ferrielectric Crystals by Coherent Spinodal Decomposition ACS Nano 2015, 9, 12365-12373.

(7) Chyasnavichyus, M.; Susner, M. A.; Ievlev, A. V.; Eliseev, E. A.; Kalinin, S. V.; Balke, N.; Morozovska, A. N.; McGuire, M. A.; Maksymovych, P. Size-Effect in Layered Ferrielectric Cuinp2s6 Appl. Phys. Lett. 2016, 109.

(8) Liu, F.; You, L.; Seyler, K. L.; Li, X.; Yu, P.; Lin, J.; Wang, X.; Zhou, J.; Wang, H.; He, H. Room-Temperature Ferroelectricity in Cuinp2s6 Ultrathin Flakes Nat. Commun. 2016, 7.

(9) Susner, M. A.; Chyasnavichyus, M.; Puretzky, A. A.; He, Q.; Conner, B. S.; Ren, Y.; Cullen, D. A.; Ganesh, P.; Shin, D.; Demir, H.; McMurray, J. W.; Borisevich, A. Y.; Maksymovych, P.; McGuire, M. A. Cation-Eutectic Transition Via Sublattice

Melting in Cuinp2s6/In4/3p2s6 Van Der Waals Layered Crystals ACS Nano 2017, 11, 7060-7073.

(10) Neumayer, S. M. E., Eugene A.; Susner, Michael A.; Tselev, Alexander; Rodriguez, Brian J.; Jesse, Stephen; Kalinin, Sergei V.; McGuire, Michael A.; Morozovska, Anna N.; Maksymovych, Petro Maksymovych; Balke, Nina Giant Negative Electrostriction and Dielectric Tunability in a Van Der Waals Layered Ferroelectric Nat. Commun. 2017, submitted.

(11) Banys, J.; Macutkevic, J.; Samulionis, V.; Brilingas, A.; Vysochanskii, Y. Dielectric and Ultrasonic Investigation of Phase Transition in Cuinp2s6 Crystals Phase Transitions 2004, 77, 345-358.

(12) Mercier, R.; Malugani, J. P.; Fahys, B.; Douglade, J.; Robert, G. Synthesis, Crystalline-Structure and Vibrational Analysis of Lithium Hexathiohypodiphosphate - Li4p2s6 J. Solid State Chem. 1982, 43, 151-162.

(13) Hood, Z. D.; Kates, C.; Kirkham, M.; Adhikari, S.; Liang, C. D.; Holzwarth, N. A. W. Structural and Electrolyte Properties of Li4p2s6 Solid State Ionics 2016, 284, 61-70.

(14) Schoop, L. M.; Eger, R.; Kremer, R. K.; Kuhn, A.; Nuss, J.; Lotsch, B. V. Structural Stability Diagram of Alnp(2)S(6) Compounds (a = Na, K, Rb, Cs; Ln = Lanthanide) Inorganic Chemistry 2017, 56, 1121-1131.

(15) Dietrich, C.; Sadowski, M.; Sicolo, S.; Weber, D. A.; Sedlmaier, S. J.; Weldert, K. S.; Indris, S.; Albe, K.; Janek, J.; Zeier, W. G. Local Structural Investigations, Defect Formation, and Ionic Conductivity of the Lithium Ionic Conductor Li4p2s6 Chem. Mater. 2016, 28, 8764-8773.

(16) Holzwarth, N. A. W.; Lepley, N. D.; Du, Y. A. Computer Modeling of Lithium Phosphate and Thiophosphate Electrolyte Materials J. Power Sources 2011, 196, 6870-6876.

(17) Rush, L. E.; Holzwarth, N. A. W. First Principles Investigation of the Structural and Electrochemical Properties of Na4p2s6 and Li4p2s6 Solid State Ionics 2016, 286, 45-50.

(18) Balke, N.; Jesse, S.; Morozovska, A. N.; Eliseev, E.; Chung, D. W.; Kim, Y.; Adamczyk, L.; Garcia, R. E.; Dudney, N.; Kalinin, S. V. Nanoscale Mapping of Ion Diffusion in a Lithium-Ion Battery Cathode Nat. Nanotechnol. 2010, 5, 749-754.

(19) Balke, N.; Maksymovych, P.; Jesse, S.; Herklotz, A.; Tselev, A.; Eom, C.-B.; Kravchenko, I. I.; Yu, P.; Kalinin, S. V. Differentiating Ferroelectric and Nonferroelectric Electromechanical Effects with Scanning Probe Microscopy ACS Nano 2015, 9, 6484-6492.

(20) Yi, W.; Savel'ev, S. E.; Medeiros-Ribeiro, G.; Miao, F.; Zhang, M. X.; Yang, J. J.; Bratkovsky, A. M.; Williams, R. S. Quantized Conductance Coincides with State Instability and Excess Noise in Tantalum Oxide Memristors Nat. Commun. 2016, 7.

(21) Morozovska, A. N.; Eliseev, E. A.; Balke, N.; Kalinin, S. V. Local Probing of Ionic Diffusion by Electrochemical Strain Microscopy: Spatial Resolution and Signal Formation Mechanisms J. Appl. Phys. 2010, 108.

(22) Morozovska, A. N.; Eliseev, E. A.; Kalinin, S. V. Electromechanical Probing of Ionic Currents in Energy Storage Materials Appl. Phys. Lett. 2010, 96.

(23) Tselev, A.; Morozovska, A. N.; Udod, A.; Eliseev, E. A.; Kalinin, S. V. Self-Consistent Modeling of Electrochemical Strain Microscopy of Solid Electrolytes Nanotechnology 2014, 25.
(24) Alikin, D. O.; Ievlev, A. V.; Luchkin, S. Y.; Turygin, A. P.; Shur, V. Y.; Kalinin, S. V.; Kholkin, A. L. Characterization of Limn2o4 Cathodes by Electrochemical Strain Microscopy Appl. Phys. Lett. 2016, 108.
(25) Balke, N.; Kalnaus, S.; Dudney, N. J.; Daniel, C.; Jesse, S.; Kalinin, S. V. Local Detection of Activation Energy for Ionic Transport in Lithium Cobalt Oxide Nano Lett. 2012, 12, 3399-3403.
(26) Jesse, S.; Balke, N.; Eliseev, E.; Tselev, A.; Dudney, N. J.; Morozovska, A. N.; Kalinin, S. V. Direct Mapping of Ionic Transport in a Si Anode on the Nanoscale: Time Domain Electrochemical Strain Spectroscopy Study ACS Nano 2011, 5, 9682-9695.
(27) Kalinin, S.; Kumar, A.; Balke, N.; McCorkle, M.; Guo, S. L.; Arruda, T.; Jesse, S. Esm of Ionic and Electrochemical Phenomena on the Nanoscale Advanced Materials & Processes 2011, 169, 30-34.
(28) Kumar, A.; Ciucci, F.; Leonard, D.; Jesse, S.; Biegalski, M.; Christen, H.; Mutoro, E.; Crumlin, E.; Shao-Horn, Y.; Borisevich, A.; Kalinin, S. V. Probing Bias-Dependent Electrochemical Gas-Solid Reactions in (Laxsr1-X)Coo3-Delta Cathode Materials Adv. Funct. Mater. 2013, 23, 5027-5036.
(29) Balke, N.; Jesse, S.; Kim, Y.; Adamczyk, L.; Tselev, A.; Ivanov, I. N.; Dudney, N. J.; Kalinin, S. V. Real Space Mapping of Li-Ion Transport in Amorphous Si Anodes with Nanometer Resolution Nano Lett. 2010, 10, 3420-3425.
(30) Amanieu, H. Y.; Thai, H. N. M.; Luchkin, S. Y.; Rosato, D.; Lupascu, D. C.; Keip, M. A.; Schroder, J.; Kholkin, A. L. Electrochemical Strain Microscopy Time Spectroscopy: Model and Experiment on Limn2o4 J. Appl. Phys. 2015, 118.
(31) Yang, S.; Wu, J. X.; Yan, B. G.; Li, L.; Sun, Y.; Lu, L.; Zeng, K. Nanoscale Characterization of Charged/Discharged Lithium-Rich Thin Film Cathode by Scanning Probe Microscopy Techniques J. Power Sources 2017, 352, 9-17.
(32) Yang, S.; Yan, B. G.; Li, T.; Zhu, J.; Lu, L.; Zeng, K. Y. In Situ Studies of Lithium-Ion Diffusion in a Lithium-Rich Thin Film Cathode by Scanning Probe Microscopy Techniques PCCP 2015, 17, 22235-22242.
(33) Yang, S.; Yan, B. G.; Wu, J. X.; Lu, L.; Zeng, K. Y. Temperature-Dependent Lithium-Ion Diffusion and Activation Energy of Li1.2co0.13ni0.13mn0.54o2 Thin-Film Cathode at Nanoscale by Using Electrochemical Strain Microscopy Acs Applied Materials & Interfaces 2017, 9, 13999-14005.
(34) Arruda, T. M.; Kumar, A.; Jesse, S.; Veith, G. M.; Tselev, A.; Baddorf, A. P.; Balke, N.; Kalinin, S. V. Toward Quantitative Electrochemical Measurements on the Nanoscale by Scanning Probe Microscopy: Environmental and Current Spreading Effects ACS Nano 2013, 7, 8175-8182.
(35) Arruda, T. M.; Kumar, A.; Kalinin, S. V.; Jesse, S. Mapping Irreversible Electrochemical Processes on the Nanoscale: Ionic Phenomena in Li Ion Conductive Glass Ceramics Nano Lett. 2011, 11, 4161-4167.
(36) Arruda, T. M.; Lawton, J. S.; Kumar, A.; Unocic, R. R.; Kravchenko, II; Zawodzinski, T. A.; Jesse, S.; Kalinin, S. V.; Balke, N. In Situ Formation of Micron-

Scale Li-Metal Anodes with High Cyclability Ecs Electrochemistry Letters 2014, 3, A4-A7.
(37) Lee, M.; O'Hayre, R.; Prinz, F. B.; Gür, T. M. Electrochemical Nanopatterning of Ag on Solid-State Ionic Conductor Rbag4i5 Using Atomic Force Microscopy Applied Physics Letters 2004, 85, 3552-3554.
(38) Shama, F. B.; Kyle, E. J.; Glennys, A. M.; Placid, M. F. Electrochemical Direct Writing and Erasing of Silver Nanostructures on Phosphate Glass Using Atomic Force Microscopy Nanotechnology 2017, 28, 065301.
(39) Jesse, S.; Baddorf, A. P.; Kalinin, S. V. Switching Spectroscopy Piezoresponse Force Microscopy of Ferroelectric Materials Appl. Phys. Lett. 2006, 88.
(40) Jesse, S.; Kalinin, S. V. Band Excitation in Scanning Probe Microscopy: Sines of Change Journal of Physics D-Applied Physics 2011, 44.
(41) Jesse, S.; Kalinin, S. V.; Proksch, R.; Baddorf, A. P.; Rodriguez, B. J. The Band Excitation Method in Scanning Probe Microscopy for Rapid Mapping of Energy Dissipation on the Nanoscale Nanotechnology 2007, 18, 435503.

TOC figure:

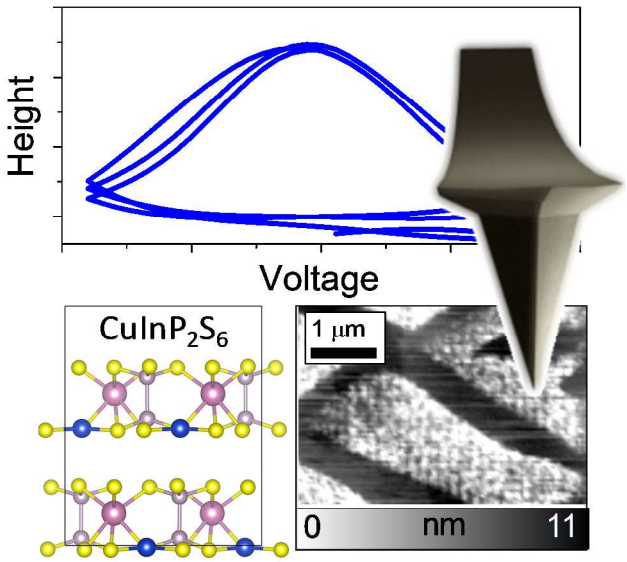

Reversible ionic motion driven by a biased scanning probe microscopy tip can be detected through volume changes in layered $CuInP_2S_6$.